Proceedings of the 28th IEEE
EMBS Annual International Conference
New York City, USA, Aug 30-Sept 3, 2006

Generation of a cardiac shape model from CT Data

Cristian Lorenz and Jens von Berg

Abstract— **In this paper we describe the generation of a geometric cardiac shape model based on cardiac CTA data. The model includes the four cardiac chambers and the trunks of the connected vasculature, as well as the coronary arteries and a set of cardiac landmarks. A mean geometric model for the end-diastolic heart has been built based on 27 end-diastolic cardiac CTA datasets and a mean motion model based on 11 multi-phase datasets. The model has been evaluated with respect to its capability to estimate the position of cardiac structures. Allowing a similarity transformation to adapt the model to image data, cardiac surface positions can be predicted with an accuracy of below 5 mm.**

I. Introduction

Diagnosis and therapy of cardiac diseases is one of the major issues of today's medicine. Imaging of the cardiac anatomy is addressed by virtually all medical imaging modalities and a considerable portion of clinical interventions concern the heart. From this context arises firstly a demand for preferably non–invasive, accurate diagnosis procedures and secondly a demand for preferably minimally invasive therapeutic procedures. Limited health–care budgets in both fields call for efficient and as much as possible automated procedures. One attempt to facilitate these requirements is the intense use of cardiac anatomical domain knowledge within the related computerized procedures.

II. Related Work

Model based cardiac evaluation procedures have been described for all 2D, 3D or 4D imaging modalities that are capable of imaging the heart, such as 3D echocardiography [6], [18], magnetic resonance tomography (MRT) [10], [8], single–photon emission computed tomography (SPECT) [3], positron emission tomography (PET), X–ray [15], and X–ray Multi–slice computed tomography (MSCT) [1]. As reviewed in [5], most work on 3D images described the left ventricle only that is clearly visible in all imaging modalities. In recent years also the right ventricle and the atria have been included in some cardiac models, extracted from cardiac MRT scans [11], [16] or MSCT [17]. Image guidance from pre–operative scans is desired during interventions at the left atrium [12]. Multi–slice computed tomography (MSCT) provides images of comparable or even higher spatial resolution than MRT and allows for a fine delineation of the four chambers as well as the trunks of the attached arteries and veins. Considerable less literature is available concerning modelling of the coronary arteries, despite their clinical importance and various attempts for automated or semi–automated segmentation. Dodge et al. reported measurements of the coronary artery locations and diameters based on bi–planar X–ray fluoroscopy data [2]. X–ray fluoroscopy is the gold–standard for coronary artery imaging and reconstruction [14].

Philips Research Europe Hamburg, Research Sector Medical Imaging Systems, 22315 Hamburg, Germany
Cristian.Lorenz@Philips.com

III. Methods

A. End-diastolic model

While the triangular multi–surface model (Fig. 1 left) was constructed in a bootstrap fashion using clinical MSCT images [17], the scheme of the coronary model was taken from [2] and it was individualized to the same MSCT training images. As manual expert surface delineation was achieved by deformation of a given model template, a Procrustes analysis could be done by point–based registration using either a rigid (6 degrees of freedom, DOF), a similarity (7 DOF), or an affine (12 DOF) transformation. The residual distances from that mean model reveal the anatomical variability of different cardiac structures beyond the global transformation of the Procrustes registration. The automated surface model individualization was realized by shape constrained deformable surface models [8]. This method used both shape similarity to the a priori model and attraction by image features in an energy minimization approach [13]. A global point–based pre–registration was achieved using the anatomical landmark set to initialise the deformable model.

B. Motion model

The motion model is based on a set of surfaces meshes of the end-diastolic model that have been adapted to patient data. Each of the N_s samples in the learning set S consists of a time series of triangular meshes covering the cardiac cycle. Each mesh is defined as a set of N_v vertices $V = v_i$ and triangular faces F referring to the vertex set:

$$S = \{T_1 \dots T_{N_s}\} \quad (1)$$

$$T = \{M_0 \dots M_{N_t}\} \quad (2)$$

$$M = \{V, F\}\,. \quad (3)$$

The number N_t of meshes in one time series is the same for all learning samples. The mesh topology, i.e. the set of triangular faces F is also the same for all meshes in a time series and for all time series. All meshes of a given time series are inherently registered since they are given in the same patient coordinate system. For the generation of a mean time series, a Procrustes registration of the learning samples T_i has to be performed, allowing a transformation A of a given transformation class. The procedure starts with one arbitrary learning sample as reference, to which all other

1-4244-0033-3/06/$20.00 ©2006 IEEE.

samples are registered by minimizing the quadratic sum of vertex distances Δ_{vv} between the reference sample and a second sample:

$$\Delta_{vv}\left(T_a, A, T_b\right) = \sum_{t=1}^{N_t}\sum_{i=1}^{N_v}\left(v_{ti}^a - A\cdot v_{ti}^b\right)^2, \qquad (4)$$

denoting the position of the i-th vertex at time t with v_{ti}. In our case, we have $N_t = 10$ meshes per time series, each mesh consisting of 7286 vertices resulting in 72860 point pairs entering the distance measure (4). The minimization problem

$$\tilde{A} = \arg\min_A\left(\Delta_{vv}\left(T_a, A, T_b\right)\right) \qquad (5)$$

is solved for an affine transformation class using a singular-value-decomposition based approach described in [7]. In order to receive a Procrustes registration of the whole learning set, we pair-wise register all samples first to a sample that has roughly a size (measured as mean distance between mesh center of mass and all vertices) close to the mean size of the learning set. The procedures results in N_s transformation matrices A_k. The vertex positions of the mean mesh time series $\bar{T}$ are given by:

$$\bar{v}_{ti} = \frac{1}{N_s}\sum_{k=1}^{N_s} A_k\cdot v_{ti}^k \qquad (6)$$

We repeat the Procrustes registration, this time using the just calculated mean mesh time series as reference. After two iterations of the procedure we did not observe any further changes in the resulting mean. In addition to the mean mesh time series of the whole learning set, we calculated N_s leave-one-out mean series. In order to avoid differences caused by arbitrary scaling during the Procrustes analysis, we used the mean series of the whole learning set as reference during the Procrustes registration for the generation of the individual leave-one-out mean series. In order to investigate the prospective value of a mean cardiac motion model, we applied the leave-one-out motion models to estimate vertex positions at a time point t_2 given the vertex positions at time point t_1 and to evaluate the difference. The procedure consists of the following steps. First the mean mesh at time t_1 is registered to the given sample mesh at t_1 allowing for the same affine transformation class as during model construction. The resulting transform A is applied to the whole time series of the model. In the second step, model vertex motion vectors $d_{t_1,t_2,i}$ are calculated as

$$d_{t_1t_2,i} = A\cdot\bar{v}_{t_2i} - A\cdot\bar{v}_{t_1i} \qquad (7)$$

Thirdly, the vertex positions of the sample mesh at time t_2 are estimated as the sample vertex positions at t_1 plus the motion vectors:

$$\hat{v}_{t_2i} = v_{t_1i} + d_{t_1t_2,i} \quad , \quad \epsilon_{t_1t_2,i} = \left|v_{t_2i} - \hat{v}_{t_2i}\right|. \qquad (8)$$

We define the *predictive value* of the motion model as the percentage of motion that can be predicted by the model:

$$P = \frac{100}{N_v}\cdot\sum_{i=1}^{N_v}\frac{\left|v_{t_2i} - v_{t_1i}\right| - \epsilon_{t_1t_2,i}}{\left|v_{t_2i} - v_{t_1i}\right|}. \qquad (9)$$

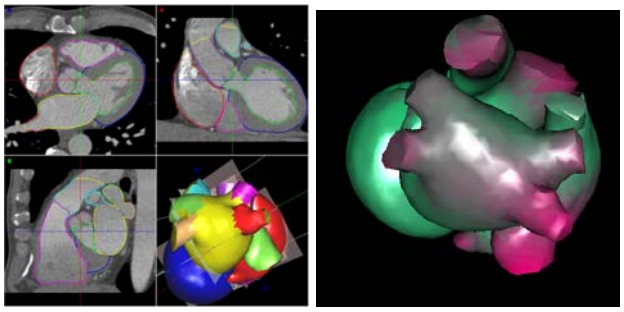

Fig. 1. Left: Multi–surface heart model constructed from an MSCT image. Right: Distribution of shape variability in the patient sample after affine co–registration.

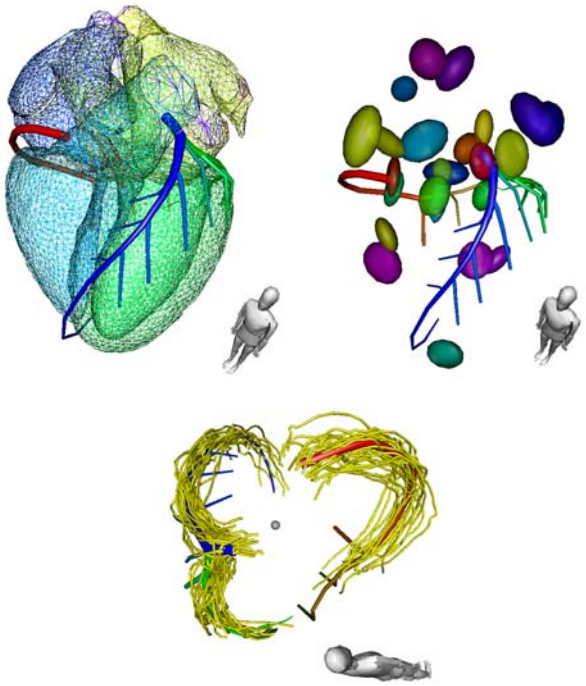

Fig. 2. Left: The mean surface model registered with the mean coronary artery model. Centre: Anatomical landmarks with their error ellipsoids registered with the mean coronary artery model. Right: Remaining variability of coronary artery centrelines.

The above formula gives the normalized difference between true motion between t_1 and t_2 and the residual estimation error $\epsilon_{t_1t_2,i}$ after application of the motion model, i.e. the amount of predicted motion.

IV. Results

A. End-diastolic model

The mean residual variability of surface vertex positions after Procrustes analysis ranged from 5.6 mm (rigid) via 4.7 mm (similarity) to 3.6 mm (affine). Most of the variability is to be observed in pulmonary vein trunks, vena cava, and right atrium (Fig. 1). The ventricles are less variable, their values range below the above mean values. These findings compare well with those of the variability of the main coronary arteries that are attached to the ventricles and

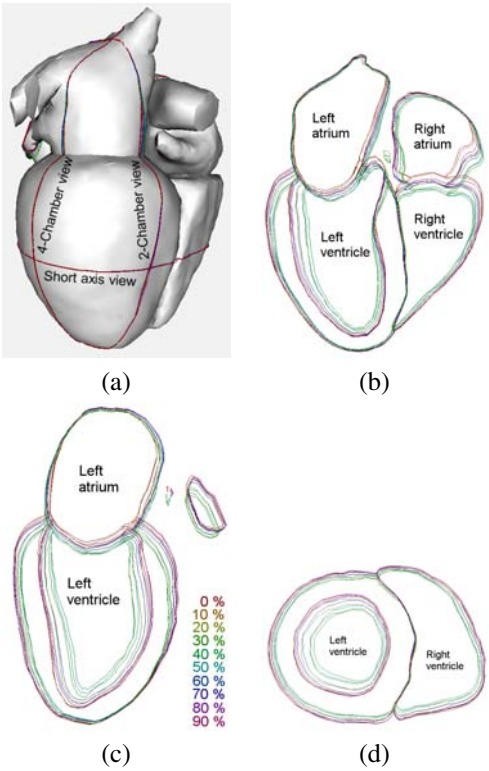

Fig. 3. (a) Surface model. (b-d) Orthogonal cuts through the mean motion model.

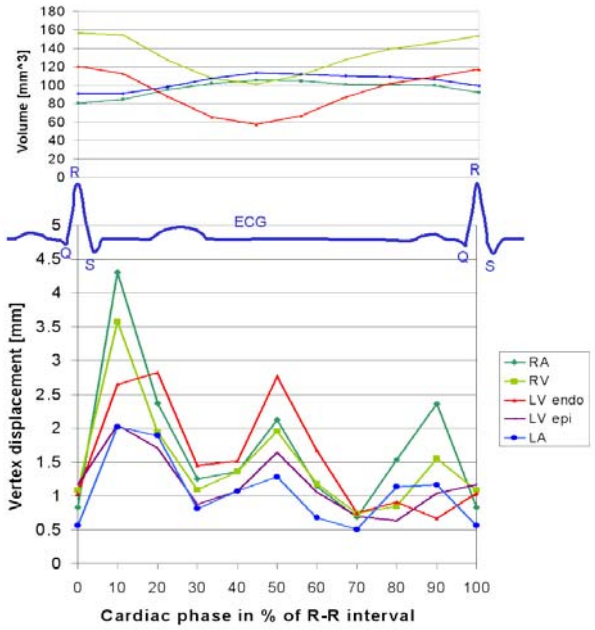

Fig. 4. From top to bottom: Volume curves of both atria and both vetricles of the mean model; typical ECG; mean vertex displacement for given sub–surfaces in mm to subsequent phase point. The three peaks represent ventricle contraction, ventricle release, and atrial contraction.

showed 3.8 mm for rigid, 3.3 mm for similarity, and 2.0 mm for affine registration as acquired in [9]. The mean residual variability over all landmark positions after Procrustes analysis was 9.1 mm (rigid), 7.7 mm (similarity), and 6.7 mm (affine). An unknown landmark position may be estimated from a set of other given well–chosen landmarks with a mean error of about 6 mm. The same holds for the localisation of the main coronary artery centrelines from some given landmarks. Figure 2 top-left shows the mean triangular surface model overlaid with the mean coronary model, which were built independently from it. The anatomical landmarks and their remaining variability after a global co–registration by the coronary centrelines are shown in Figure 2 top-right as error ellipsoids in the model co–ordinate system. Figure 2 bottom shows the variability of coronary artery centrelines manually delineated in the patient sample after co–registration of their corresponding cardiac surfaces. The coronary artery model was adapted to minimise the summed distance to all these individual centrelines. A mean surface model built from a subset of patients and adapted to the remaining images yielded a mean distance of 3.1 mm to reference expert data after the global landmark–based pre–registration (similarity). The distance of vertex v_1 in surface s_1 to surface s_2 was calculated determining the closest point in a local patch surrounding the corresponding vertex v_2 in s_2. Such a patch included all neighbour triangles with a maximal triangle distance of 3 from v_2. The subsequent automatic deformable surface adaptation improved this result to a distance of 1.1 mm averaged over all subjects and all anatomical regions. When the globally pre–registered model is used to estimate the main coronary position, a mean centreline distance of 5.4 mm (similarity) or 5.2 mm (affine) can be observed to the manual delineated centrelines.

B. Motion model

The procedure described above leads to a mean motion model generated from a learning set of 11 samples and in 11 leave-one-out models generated from reduced sets of 10 learning samples each. Consequently, the results relate on the one hand to the general properties of the overall mean model and on the other hand to the predictive value of the leave-one-out models applied to the left out sample. Figure (3a) shows a 3D rendering of the cardiac shape model that was used as basis for the motion model. On the surface, 3 orthogonal cut-planes are indicated that define the geometries of the mesh cut lines depicted in Figures (3b-d). Figure (3b) shows a four-chamber view cutting through left and right ventricle and left and right atrium, Figure (3c) shows a two chamber view, cutting through left ventricle and left atrium and Figure (3d) shows a short-axis view, cutting through left and right ventricle. In all three cut planes the mean model meshes of all 10 phases are depicted showing the temporal variation of the mesh. Clearly visible is the expected strong motion of the endocardium of the left ventricle. Interesting however is the comparatively strong motion of the right atrium, which can be partially explained by passively following the motion of the connected ventricles. Figure 4 shows quantitatively the motion of the cardiac surfaces and volumes over the cardiac cycle. The lower graph depicts the mean Euclidean distance

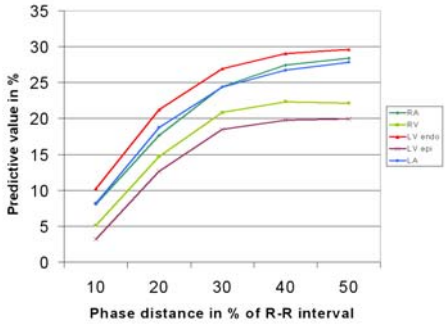

Fig. 5. Predictive value of the motion model.

between the position of a vertex at subsequent phase-points for different sub–surfaces. The upper graph shows the volume curves of the four chambers. In addition, a typical ECG signal is shown as reference. Note the minimum of motion at the late diastole, corresponding to the empirically found value for optimal MSCT coronary artery imaging at about 70% cardiac phase. The graph again shows the strong motion at the right atrium which is the cause for frequent motion artefacts when imaging the right coronary artery. In addition to minimal motion at 70% the graphs shows a second minimum at $30-40\%$ corresponding to end-systole. In order to assess the potential of the method to predict the cardiac motion for an individual case, we calculated the *predictive value* as defined in (9) for all t_1, t_2 combinations and for all leave one-out-models. All experiments with the same phase distance between t_1 and t_2 (taking into account the cyclic nature of the process) have been merged for a concise presentation. The most predictable surface is the endocardium of the left ventricle with a value of up to 30%.

V. Discussion

A statistical model of the human heart was presented that covers surfaces of all four chambers and the attached vessel trunks, the centrelines of the three main coronary arteries, and a set of 25 cardiac anatomical landmarks. The variability of cardiac substructures in a sample set of 27 end–diastolic multi–slice CT images was analysed. The model was mainly used to estimate shape and position of cardiac substructures by the use of other cardiac substructures (e.g. surfaces by landmarks, coronaries by surfaces). The surfaces may be also automatically deformed to fit the respective image boundaries. The application of the surface model for fully automatic cardiac analysis is currently employed [4]. In addition to the end-diastolic shape model, a mean cardiac motion model was created on the basis of 11 multi-phase data sets. Volume curves and local velocity measures of this mean model were presented. In a leave–one–out test the prediction of the shape of an unknown phase point based on a given individual shape of a different phase point and the mean motion model was evaluated. Up to 30% of the individual cardiac motion can be predicted by the mean motion model (see Figure 5).

Acknowledgements

We would like to thank our colleagues from Philips Research in Aachen and Philips Medical Systems in Best, Cleveland and Haifa for their kind support and many fruitful discussions. We also would like to thank J. T. Dodge for kindly making available updated position measurements of the coronary arteries.

References

[1] T. Chen, D. Metaxas, and L. Axel. 3D cardiac anatomy reconstruction using high resolution CT data. In *Proc. of MICCAI*, pages 411–418. Springer–Verlag, 2004.

[2] J. T. Dodge, B. G. Brown, E. L. Bolson, and H. T. Dodge. Intrathoracic spatial location of specified coronary artery segments on the normal human heart. Applications in quantitative arteriography, assessment of regional risk and contraction, and anatomic display. *Circulation*, 78:1167–1180, 1988.

[3] L. Dornheim, K. Tönnies, and K. Dixon. Automatic segmentation of the left ventricle in 3D SPECT data by registration with a dynamic anatomical model. In *Proc. of MICCAI*, pages 335–342. Springer–Verlag, 2005.

[4] Olivier Ecabert, Jochen Peters, Cristian Lorenz, Jens von Berg, Mani Vembar, Krishna Subramanyan, and Jürgen Weese. Towards automatic full heart segmentation in computed–tomography images. In *Computers in Cardiology*, 2005.

[5] A. F. Frangi, W. J. Niessen, and M. A. Viergever. Three–dimensional modeling for functional analysis of cardiac images: A review. *IEEE TMI*, 20:2–25, 2001.

[6] O. Gérard, A. Collet Billon, J.-M. Rouet, M. Jacob, M. Fradkin, and C. Allouche. Efficient model–based quatification of left ventricular function in 3D echocardiography. *IEEE Trans. Med. Imag.*, 21(9):1059–1068, 2002.

[7] G. Golub and C. van Loan. *Matrix Computation*. John's Hopkins University Press, Baltimore, MD, USA, 3rd edition, 1996.

[8] M. R. Kaus, J. von Berg, J. Weese, W. Niessen, and V. Pekar. Automated segmentation of the left ventricle in cardiac MRI. *Med. Img. Anal.*, 8:245–254, 2004.

[9] C. Lorenz, J. von Berg, T. Bülow, S Renisch, and S. Wergandt. Modeling the coronary artery tree. In *Proc. of Shape Modeling International 2004*, pages 354–357. IEEE Comput. Soc, 2004.

[10] M. Lorenzo-Valdés, G. I. Sanchez-Ortiz, R. Mohiaddin, and D. Rueckert. Atlas-based segmentation and tracking of 3D cardiac MR images using non–rigid registration. In *Poc. of MICCAI*, pages 642–650. Springer, 2002.

[11] J. Lötjönen, S. Kivistö, J. Koikkalainen, D. Smutek, and K. Lauerma. Statistical shape model of atria, ventricles and epicardium from short– and long–axis MR images. *Med. Img. Anal.*, 8:371–386, 2004.

[12] E. M. Marom, J. E. Herndon, Y. H. Kim, and H. P. McAdams. Variations in pulmonary venous drainage to the left atrium: Implications for radiofrequency ablation. *Radiology*, 230(3):824–829, 2004.

[13] T. McInerney and D. Terzopoulos. Deformable models in medical image analysis: A survey. *Med. Img. Anal.*, 1(2):91–108, 1996.

[14] B Movassaghi, V Rasche, M Grass, M A Viergever, and W J Niessen. A quantitative analysis of 3–D coronary modeling from two or more projection images. *IEEE Transaction on medical imaging*, 23(912):1571–1531, 2004.

[15] E. Oost, G. Koning, M. Sonka, H. C. Reiber, and B. P. F. Lelieveldt. Automated segmentation of X–ray left ventricular angiograms using multi–view active appearance models and dynamic programming. In Frangi, Radeva, Santos, and Hernandez, editors, *LNCS 3504, FIMH*, pages 23–32. Springer–Verlag, 2005.

[16] R. Pilgram, K. D. Fritscher, and R. Schubert. Modeling of the geometric variation and analysis of the right atrium and right ventricle motion of the human heart using PCA. In *Proc. of CARS*, pages 1108–1113. Elsevier, 2004.

[17] J. von Berg and C. Lorenz. Multi–surface cardiac modelling, segmentation, and tracking. In Frangi, Radeva, Santos, and Hernandez, editors, *LNCS 3504, FIMH*, pages 1–11. Springer–Verlag, 2005.

[18] V. Zagrodsky, V. Walimbe, C. R. Castro-Pareja, Jian Xin Qin, Jong-Min Song, and R. Shekhar. Registration-assisted segmentation of real-time 3-D echocardiographic data using deformable models. *IEEE Trans. Med. Imag.*, 24(9):1089–1099, 2005.